




Characterization and genomics analysis of phage PGX1 against multidrug-resistant enterotoxigenic *E. coli* with in vivo and in vitro efficacy assessment

Dayue Hu^{1,2,3}, Ping Qian^{1,2,3*}, Dongyang Gao^{1,2,3}, Xinxin Li^{1,2,3}, Linkang Wang^{1,2,3}, Hongyue Ji^{1,2,3}, Shuang Wang^{1,2,3} and Xiangmin Li^{1,2,3*} 

Abstract

Enterotoxigenic *E. coli* is one of the bacterial pathogens contributing to the global resistance crisis in public health and animal husbandry. The problem of antibiotic resistance is becoming more and more serious, and phage is considered one of the potential alternatives to antibiotics that could be utilized to treat bacterial infections. Our study isolated and identified a lytic phage PGX1 against multidrug-resistant enterotoxigenic *E. coli* EC6 strain from sewage. The phage lysis profile revealed that PGX1 exhibited a lytic effect on multidrug-resistant enterotoxigenic *E. coli* strains of serotype O60. Through phage whole genome sequencing and bioinformatics analysis, PGX1 was found to be the class *Caudoviricetes*, family *Autographiviridae*, genus *Teseptimavirus*. The length of the PGX1 genome is about 37,009 bp, containing 54 open reading frames (ORFs). Notably, phage PGX1 lacks any lysogenic-related genes or virulence genes. Furthermore, phage PGX1 demonstrates strong adaptability, tolerance, and stability in various pH (pH4-10) and temperatures (4–40°C). The in vivo and in vitro tests demonstrated that phage PGX1 significantly removes and inhibits the formation of multidrug-resistant EC6 biofilm and effectively controls the *Galleria mellonella* larvae and enterotoxigenic *E. coli* EC6 during mice infection. In conclusion, the above findings demonstrated that phage PGX1 may be a novel antimicrobial agent to control multidrug-resistant *E. coli* infections.

Keywords Enterotoxigenic *E. coli*, Multidrug-resistant bacteria, Phage PGX1

Communicated by Yuan Liu.

*Correspondence:

Ping Qian
qianp@mail.hzau.edu.cn

Xiangmin Li
lixiangmin@mail.hzau.edu.cn

¹ National Key Laboratory of Agricultural Microbiology, Hubei Hongshan Laboratory, Huazhong Agricultural University, Wuhan 430070, China

² The Cooperative Innovation Centre for Sustainable Pig Production, Huazhong Agricultural University, Wuhan 430070, China

³ College of Veterinary Medicine, Huazhong Agricultural University, Wuhan 430070, China

Introduction

Enterotoxigenic *E. coli* (EPEC) is a prevalent foodborne and zoonotic pathogen causing diarrhea in humans and young animals, potentially leading to death in severe cases (Abri et al. 2019; Hosangadi et al. 2019). The adhesive function of K88 fimbriae adhesins is one of the crucial factors contributing to EPEC disease, and the infected newborn animals often die from severe watery diarrhea and rapid dehydration, resulting in high rates of morbidity and mortality (Gresse et al. 2017). The adhesion of EPEC is a critical step in its pathogenic process, which facilitates bacterial attachment to object surfaces, colonization, and biofilm formation (Lu et al. 2019).



© The Author(s) 2024. **Open Access** This article is licensed under a Creative Commons Attribution 4.0 International License, which permits use, sharing, adaptation, distribution and reproduction in any medium or format, as long as you give appropriate credit to the original author(s) and the source, provide a link to the Creative Commons licence, and indicate if changes were made. The images or other third party material in this article are included in the article's Creative Commons licence, unless indicated otherwise in a credit line to the material. If material is not included in the article's Creative Commons licence and your intended use is not permitted by statutory regulation or exceeds the permitted use, you will need to obtain permission directly from the copyright holder. To view a copy of this licence, visit <http://creativecommons.org/licenses/by/4.0/>. The Creative Commons Public Domain Dedication waiver (<http://creativecommons.org/publicdomain/zero/1.0/>) applies to the data made available in this article, unless otherwise stated in a credit line to the data.

Bacterial biofilms can enhance bacterial resistance to the external environment and possess inherent resistance and immunity to antibiotics (Bowler 2018; Hathroubi et al. 2017; Roy et al. 2018). Furthermore, the bacteria encapsulated in biofilms are in a low-energy state that is not sensitive to antibiotics, so antibiotics cannot completely kill the bacteria, leading to the increase of bacterial tolerance, the generation of drug-resistant mutants, and the development of chronic infectious diseases (Harms et al. 2016; Levin-Reisman et al. 2017; Zalis et al. 2019). Therefore, once bacteria form a persistent biofilm, it becomes difficult to remove. With bacterial-resistant mutants continuing to emerge, the crisis of antimicrobial resistance (AMR) is becoming increasingly serious, constantly threatening the survival and well-being of animals and humans (Antimicrobial Resistance 2022). Therefore, finding a solution to the drug resistance dilemma is imperative.

Phages offer many advantages, such as strong specificity, fast self-reproduction, low stress on the body, non-toxic to mammalian cells, and do not cause extensive damage to the normal flora in the body (Gordillo Altamirano and Barr 2019; Moghadam et al. 2020). Consequently, phages are also considered one of the potential approaches to treat the infection of superbugs during clinical trials (Chan and Chang 2022; Mohammadi et al. 2023; Ooi et al. 2019; Prazak et al. 2022; Waters et al. 2017; Yin et al. 2017). Furthermore, multiple research findings have also shown that phages successfully prevent emerging bacterial resistance by removing bacterial biofilm (Chaudhary et al. 2022; Goodarzi et al. 2021; Jiang et al. 2022; Soontarach et al. 2022).

This study found that PGX1 was a virulent phage capable of lysing multidrug-resistant *E. coli* strains of serotype O60. Subsequently, we evaluated the potential application of phage PGX1 in controlling multidrug-resistant ETEC via the *G. mellonella* larvae and mice models of systemic infection.

Results

Virulence genes and drug resistance of the isolated *E. coli* strains

The *E. coli* strains were isolated from the intestinal feces of piglets with diarrhea and sewage, named EC_n (n represents a natural number), and analyzed the virulence genes and drug resistance. We found that eight *E. coli* strains (EC2, EC6, EC7, EC22, EC23, EC30, EC39 and EC40) had a unique virulence FaeG gene belong to ETEC K88 (Fig. 1B and S1). The 8 *E. coli* clinical isolates and *E. coli* 15857 stored in the laboratory were resistant to more than twenty antibiotics, including Ampicillin, Kanamycin, Chloramphenicol, and Cefoperazone (Fig. 1, Table S1). The results suggested that the nine *E. coli* strains

(EC2, EC6, EC7, EC22, EC23, EC30, EC39, EC40 and 15857) were multidrug-resistant bacteria.

Isolation and morphology of phage

Phage PGX1 was successfully isolated and purified from sewage using ETEC EC6 as the host strain by the double-layer plate method. On the plates, the purified phage PGX1 plaques appeared as circular plaques with a diameter of about 3.0 ± 0.5 mm (n=10), a distinct boundary, and no halo ring (Fig. 2A). Electron microscope images revealed that the head diameter of phage PGX1 was approximately 35.0 ± 1.2 nm (n=10), and the short tail was about 10.0 ± 0.8 nm (n=10) (Fig. 2B).

Biological characteristics analysis

The phage titer was highest at 1 MOI (multiplicity of infection), indicating that the optimal MOI of phage PGX1 against ETEC EC6 was 1 (Fig. 2C). The result of the one-step growth curve showed little change in the titer of PGX1 during the first 10 min, followed by a rapid increase to a higher titer within approximately 30 min (Fig. 2D). Therefore, we concluded that PGX1 has a relatively short latent period of about 10 min, and a lysis phase about 30 min. Additionally, the results of the heat and pH stability assay showed that the titer of phage PGX1 remained relatively stable from 4°C to 50°C and from pH 4 to pH 10 (Fig. 2E and F). However, the titer began to sharply decline with the temperature increasing above 50°C, and no phage appeared at 70°C (Fig. 2E). Meanwhile, PGX1 was inactivated in environments of pH 2 and 12 (Fig. 2F).

The host range and EOP of phage PGX1 were measured using the spot titer assay on double-layer agar plates containing 52 different strains (Table S2). We discovered that PGX1 could lyse nine multidrug-resistant *E. coli* strains of serotype O60, while it did not lyse other strains. The EOP of the phage on the nine *E. coli* strains were found to be 1%, 100.0%, 2.0%, 36.4%, 8.6%, 37.3%, 4.5%, 1.4% and 40.9% on EC2, EC6, EC7, EC22, EC23, EC30, EC39, EC40 and 15857 plates, respectively (Fig. 3A and B). The phage lysis curve showed that phage PGX1 at different MOI could rapidly lyse host bacteria within 1 h, reducing the absorbance of bacteria to the lowest detection limit (Fig. 3C). However, with the increase of time, the bacterial mutants also increased, and the growth density of bacterial mutants at MOI of 10 was higher than that at MOI of 0.01 (Fig. 3C).

Genomic characteristics and alignment analysis of phage PGX1

The phage PGX1 genome is a double-stranded DNA of 37,009 bp with 48% GC, containing 54 ORFs (Fig. 4A). Through the BLASTp alignment analysis of the ORFs, 40

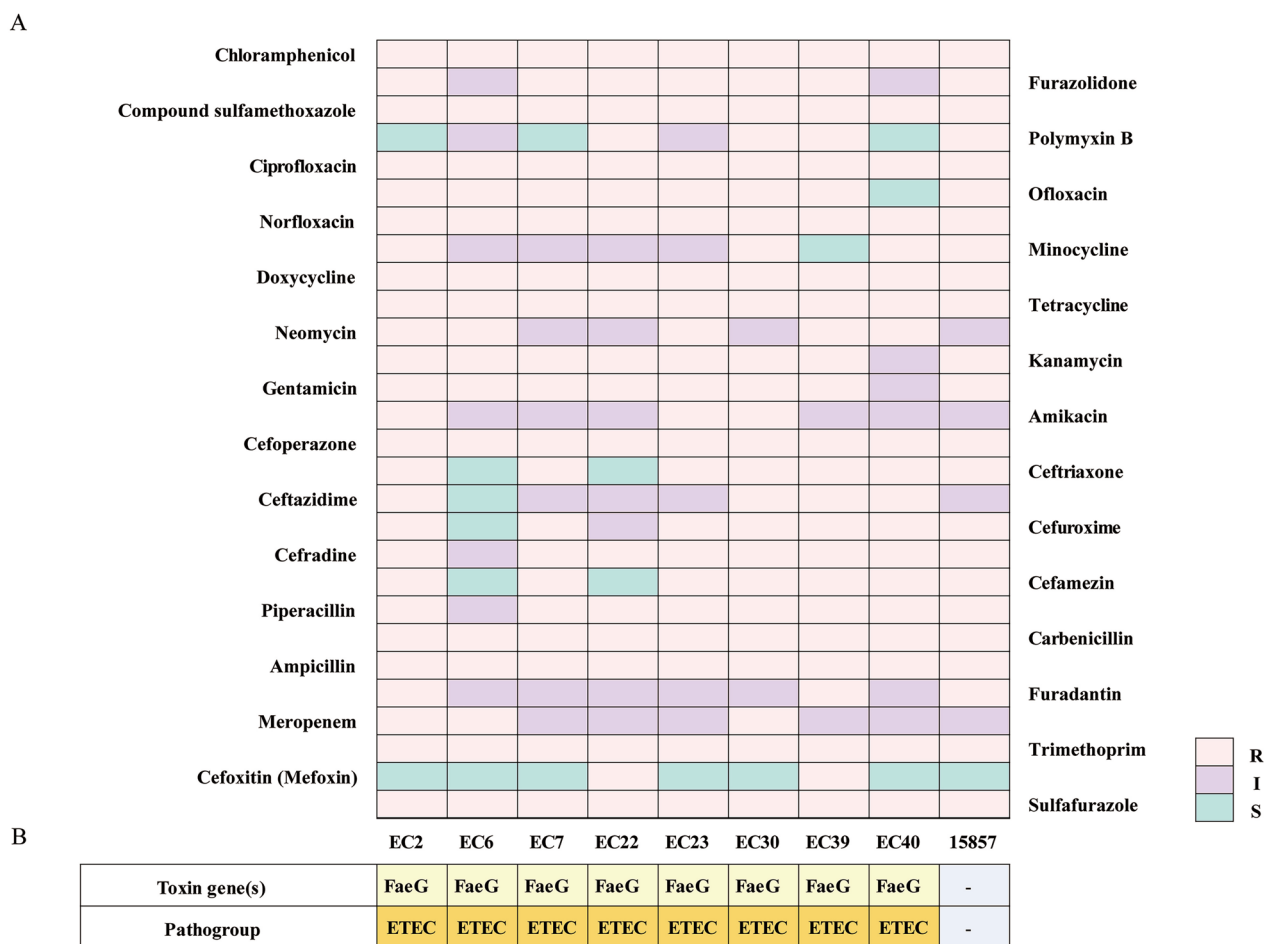


Fig. 1 The drug resistance and virulence genes of *E. coli* isolates. **A** Anti-resistance profile of representative *E. coli* isolates. Antibiotic resistance: pink means resistant (R), purple means insensitive (I), and green means susceptible (S). The tested antibiotics included Chloramphenicol, Compound Sulfamethoxazole, Ciprofloxacin, Norfloxacin, Doxycycline, Neomycin, Gentamicin, Cefoperazone, Ceftazidime, Cefradine, Piperacillin, Ampicillin, Meropenem, Cefoxitin (Mefoxin), Furazolidone, Polymyxin, Ofloxacin, Minocycline, Tetracycline, Kanamycin, Amikacin, Ceftriaxone, Cefuroxime, Cefamezin, Carbenicillin, Furadantin, Trimethoprim and Sulfafurazole. **B** Corresponding virulence genes and typing of the tested multidrug-resistant *E. coli* isolates. Yellow indicates the presence of the FaeG gene, orange indicates belonging to ETEC, and blue represents the absence of any of the tested virulence genes, making it impossible to determine the group to which it belongs

ORFs were classified as functional proteins, and the other ORFs were categorized as hypothetical proteins (Fig. 4A). More detailed annotation and alignment information is provided in Supplementary Table S3. Through the analysis of the phage PGX1 genome, it was found that PGX1 did not contain any lysogenic-related genes, tRNA genes, drug-resistant genes, virulence genes, or transmembrane topology.

The homologous amino acid sequences of terminal large subunits were identified from the GenBank database using BLASTp analysis, then based on this constructed the phylogenetic tree. BLASTp analysis showed that the terminal large subunits of phage PGX1 shared 98.31% identity (99% sequence coverage) with *Enterobacteria* phage AH67C600_Q5 (UAW07012.1), and 97.97%

identity (99% sequence coverage) with *Escherichia* phage C5 (YP_009795847.1). The result of the phylogenetic tree showed that the terminal large subunits of *E. coli* phage PGX1, *Enterobacteria* phage AH67C600_Q5, and *Escherichia* phage C5 belong to the same branch, indicating they are homologous (Fig. 4B).

Furthermore, the genomic alignment of PGX1 with GenBank database sequences using BLASTn revealed that phage PGX1 had a high similarity to known phages (Data not shown). ANI values of eleven phages with high similarity were calculated by the online analysis at the website of JSpeciesWS and the homologous evolution relationship was analyzed by TBtools software. The results revealed that the phage PGX1 had more than 80% genome-wide similarity with other phages, among which

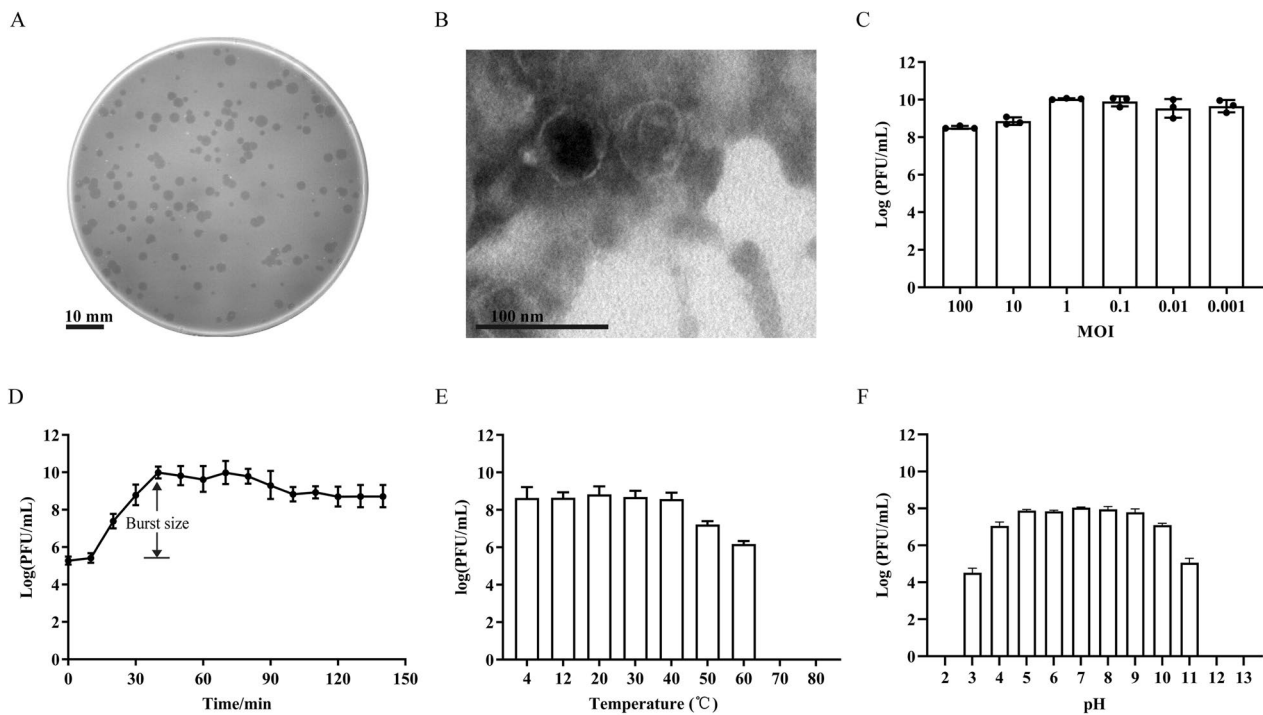


Fig. 2 Biological characteristics of phage PGX1. **A** The plaque morphology of phage PGX1 on the double-layer plate, the scale bar represents 10 mm. **B** Transmission Electron Microscopic (TEM) image of phage PGX1, the scale bar represents 100 nm. **C** The optimal MOI (multiplicity of infection) test of phage PGX1. **D** The one-step growth curve of phage PGX1. **E** The thermostability and **F** pH stability of PGX1, the data points are the logarithmic value of phage titers measured after incubation of phage at different temperatures and pH for 1 h. All assays were repeated three times, and each point represents the means \pm SD from all experiments

A

Strain	EC2	EC3	EC6	EC7	EC16	EC17	EC18	EC19	EC20	EC21	EC22	EC23	EC24	EC30	EC39	EC40	14073
Sensitivity	(1.0)	-	(100.0)	(2.0)	-	-	-	-	-	-	(36.4)	(8.6)	-	(37.3)	(4.5)	(1.4)	-
Strain	15857	18699	18701	18703	18704	18705	18706	18708	18709	18710	18711	18712	18714	18715	18716	18718	18719
Sensitivity	(40.9)	-	-	-	\pm	\pm	-	-	-	-	\pm	-	-	-	-	-	-

 Productive infection (EOP %)
 No infection
 Non-productive infection

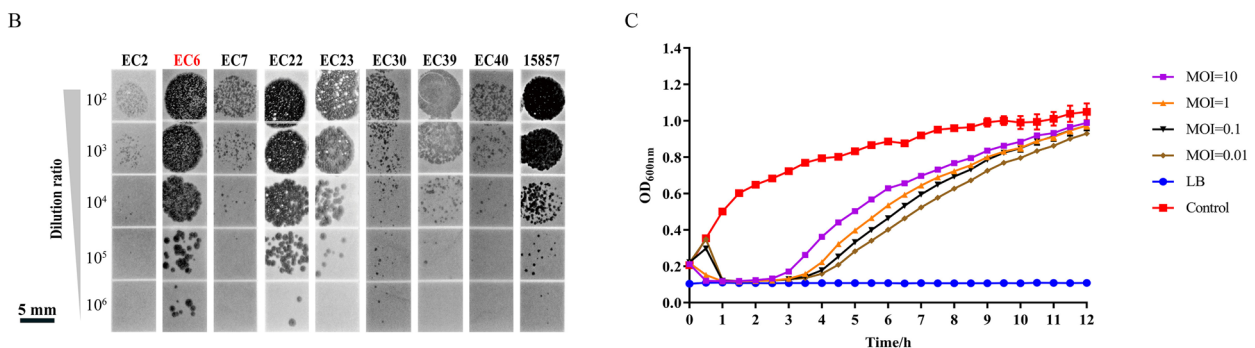


Fig. 3 Host range of phage PGX1 and lysis kinetics. **A** Host spectrum and lytic efficiency of phage PGX1 against different bacterial strains. **B** The titer of phage PGX1 on different bacterial plates, the scale bar represents 5 mm **C** Lysis kinetics curves of phage PGX1 against *E. coli* EC6 at different MOI (10, 1, 0.1, and 0.01). The tests were repeated three times, and each point represents the means \pm SD from all experiments. MOI, multiplicity of infection

the highest similarity was 91.77% with *Escherichia* phage C5 (Fig. 5A). The homology linearization analysis of the whole genome by Easyfig V. 2.2.5 software showed that the phage PGX1 tail filament protein (ORF49) was significantly different from the other four *Escherichia* phages (C5, 13A, T7 and PHB19) (Fig. 5B). Therefore, based on the above results of genome analysis, the phage PGX1 belongs to the class *Caudoviricetes*, family *Autographiviridae*, genus *Teseptimavirus* according to the ICTV classification criterion.

The efficiency of phage PGX1 removal and inhibition of biofilms in vitro

The efficiency of phage PGX1 in removing the ETEC EC6 biofilms was evaluated using crystalline violet staining. We found that the OD_{590nm} values of the phage-treated group were approximately 0.32, 0.30 and 0.34, and those of the control group were 0.96, 0.63 and 0.58 at 24, 48 and 72 h, respectively, and the differences were statistically significant by T-tests ($P < 0.01$) (Fig. 6A). This indicated that treatment with phage PGX1 had a significant removal effect on the biofilm formed by EC6. Furthermore, the results of STYO™ 9 staining showed that the fluorescence integrated density of the PGX1 treatment (approximately 4.8×10^6 AU) was much lower than that of the control (approximately 1×10^9 AU), with a statistically significant ($P < 0.0001$) (Fig. 6C and D). As expected, this further indicated the positive scavenging effect of phage on biofilm.

As shown in Fig. 6B, the OD_{590nm} values of the PGX1-treated groups were 0.66, 0.47 and 0.26, and the control groups were 1.19, 1.25 and 0.75 at 24, 48 and 72 h, respectively ($P < 0.01$). The results showed that phage PGX1 had a continuous inhibitory effect on the formation of *E. coli* EC6 biofilm within 72 h (Fig. 6B). In summary, the phage PGX1 was able to inhibit and remove the biofilm formed by ETEC EC6 effectively.

Bactericidal efficacy of phage PGX1 on the *G. mellonella* larvae model

First, the safety of purified PGX1 by CsCl₂ gradient was evaluated in *G. mellonella* larvae. It was found that the

survival rate of *G. mellonella* larvae was 100% when injected with different concentrations of purified phage PGX1 (5×10^7 , 5×10^6 , 5×10^5 , 5×10^4 , 5×10^3 and 5×10^2 PFU), which was comparable to that of the PBS group (Fig. S2B). This finding suggests that the purified phage PGX1 is safe for *G. mellonella* larvae when injected at concentrations below 5×10^7 PFU (Fig. S2B). Meanwhile, to determine the LD₅₀ of *E. coli* EC6, the *G. mellonella* larvae were challenged with different doses (CFU) of EC6 in 25 µL and observed for 48 h. As shown in Fig. S2A, the LD₅₀ of EC6 against *G. mellonella* larvae was 10^5 CFU. We next assessed the protective effects of various MOI phage PGX1 on EC6 infection after 1 h and 3 h to identify the effectiveness of the phage PGX1 in preventing enterotoxigenic *E. coli* EC6 infection in vivo.

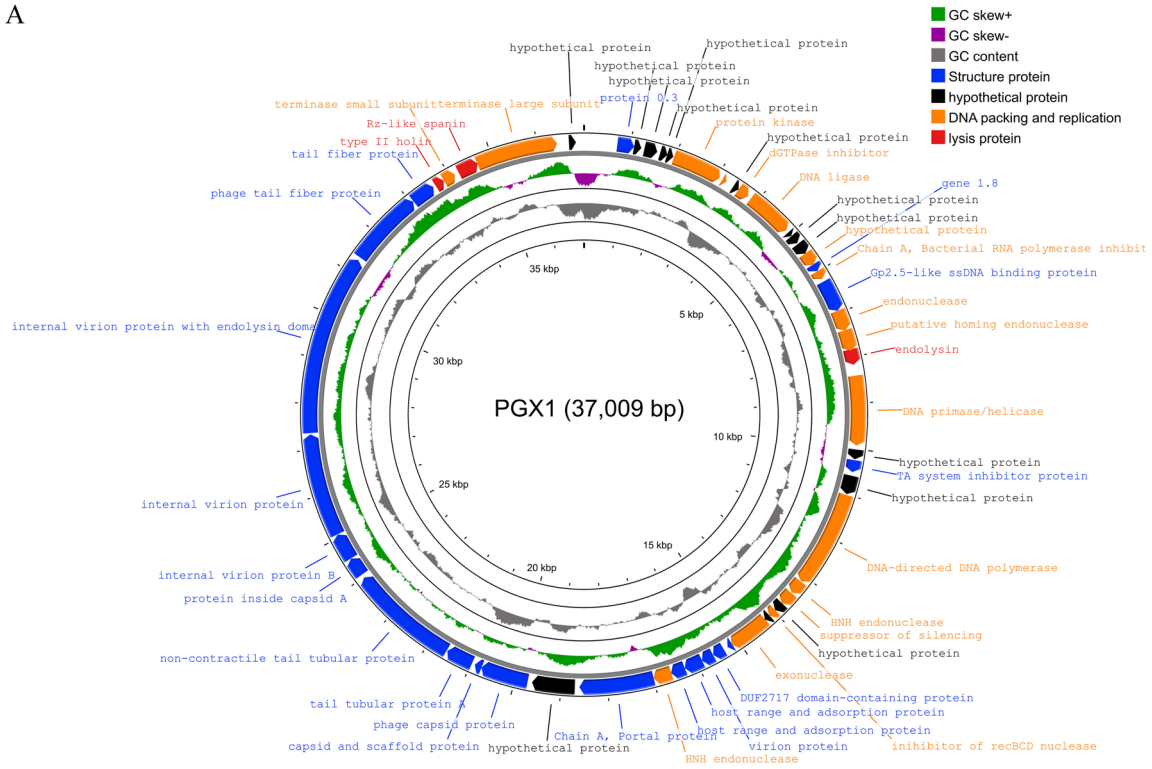
When purified phage PGX1 was pre-injected for 1 h at different MOI (100, 10, 1, 0.1, 0.01 and 0.001), it was found that phage PGX1 provided more than a 50% protective efficiency against EC6-infected *G. mellonella* larvae. When MOI was 1, 0.1 and 0.01, respectively, the protections were more than 90% against EC6-infected *G. mellonella* larvae within 96 h (Fig. 7A). However, the protective efficiency of phage PGX1 was attenuated when administrating to *G. mellonella* larvae injected with EC6 more than 3 h. The phage PGX1 provided over 50% protection against EC6 infection at MOI of 100, 10 and 0.001 within 96 h (Fig. S2C). In addition, when PGX1 was injected at an MOI of 1, the survival rate of *G. mellonella* larvae was only 30%, and the phage PGX1 did not appear to have a protective effect (Fig. S2C).

To assess the therapeutic effect of phage PGX1 against EC6-infected *G. mellonella* larvae, the *G. mellonella* larvae were challenged by EC6 at LD₅₀, injected PGX1 with different MOI after 1 and 3 h, and then the survival rates were continuously monitored. The results exhibited that the phages had a therapeutic effect of more than 50% on the *G. mellonella* larvae at MOI of 0.1, 10 and 100. Interestingly, when injected with PGX1 at an MOI of 0.1, phage PGX1 showed the best therapeutic effect with 100% survival on the *G. mellonella* larvae infected with EC6 (Fig. 7B). On the contrary, when PGX1 was injected

(See figure on next page.)

Fig. 4 Genomic characteristics of phage PGX1. **A** Circular genomic map of phage PGX1. The map is scaled in kb, and it shows GC skew (green and purple), the GC content (gray inner rings), and the predicted ORFs (the outer ring with different colored arrows). Orange arrows represent DNA packing and replication-related sequences; blue arrows indicate structural proteins; red arrows indicate lysis proteins and black arrows represent hypothetical proteins. **B** Phylogenetic analysis of PGX1 labeled in red and other phages was conducted using the protein sequences of the terminal large subunits

A



B

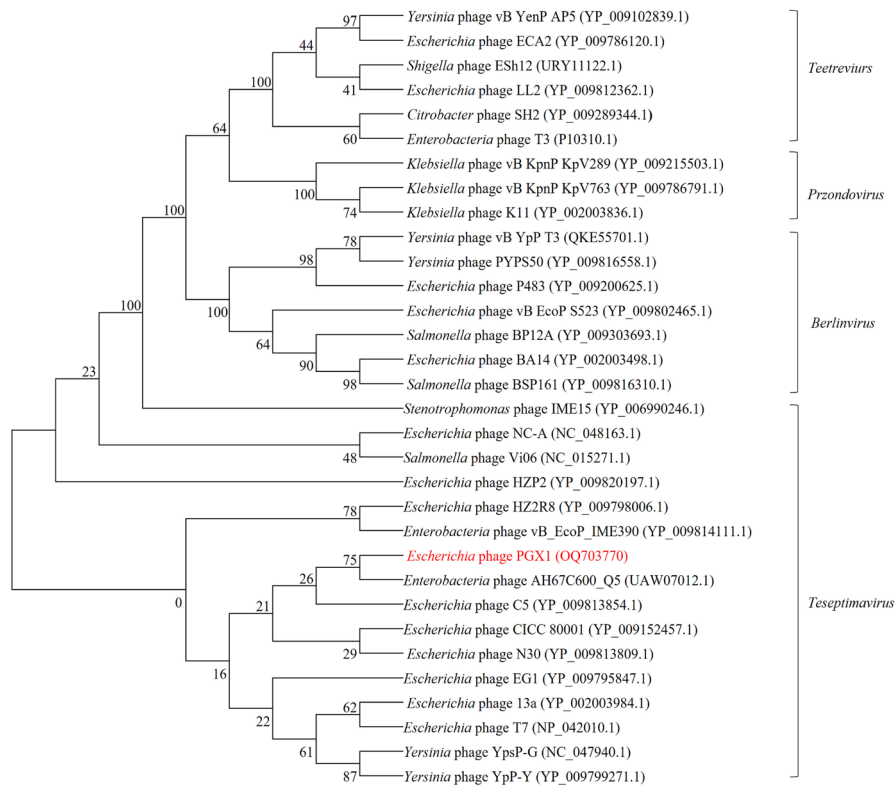


Fig. 4 (See legend on previous page.)

3 h after EC6 infection, the survival rate at an MOI of 0.1 was only 40% (Fig. S2D).

Therapeutic efficacy of phage in mice

Mice were first challenged with 150 μ L ETEC EC6 (5×10^8 CFU) via intraperitoneal injection (i.p.) to evaluate the therapeutic effect of phage in mice. Then, mice were treated with 150 μ L phage PGX1 at MOI of 0.1 (5×10^7 CFU) at 1 and 3 h after infection with EC6. Through continuous monitoring for 7 d, it was found that the survival rate of the challenge group was less than 40% within 48 h, while the survival rate of the mice in the phage treatment groups was higher than 60%. The survival rate of the mice treated with phage PGX1 at 1 h after the challenge could reach more than 80%, which was better than the phage PGX1 treatment group at 3 h (Fig. 8A). Moreover, the bacterial loads in the liver, spleen, kidney, and ileum of the PGX1-treated mice were extremely significantly lower than those of the challenge mice at 48 h after infection ($P < 0.001$) (Fig. 8B). And in the jejunal tissue, the bacterial load of the phage delayed treatment for 1 h was significantly lower than that of the challenge group ($P < 0.05$) (Fig. 8B). These findings suggested that phage PGX1 had a positive therapeutic effect on mice infected with multidrug-resistant ETEC EC6, which could reduce the colonization of multidrug-resistant ETEC EC6 in mouse tissues and organs, and the effect of phage PGX1 treatment at 1 h post-challenge was better than that at 3 h post-challenge.

Discussion

Suppose the development trend of antimicrobial resistance (AMR) cannot be effectively curbed. In that case, the number of deaths caused by "superbugs" will continue to increase, and the crisis of antibiotic resistance may force humanity to return to the era before the use of antibiotics when dealing with epidemics and pandemics (Lewis 2020). Currently, phages play a crucial role in treating "superbug" infections (Alsaadi et al. 2021; El-Shibiny et al. 2017).

In our study, the phage PGX1 had typical characteristics of phage of the genus *Teseptimavirus*, such as a head and a non-contraction tail, clear plaques on the host bacteria double-layer plate, a short incubation period, and strong lytic activity without lysogenization of the host bacteria (Dion et al. 2020; McDougall et al. 2020).

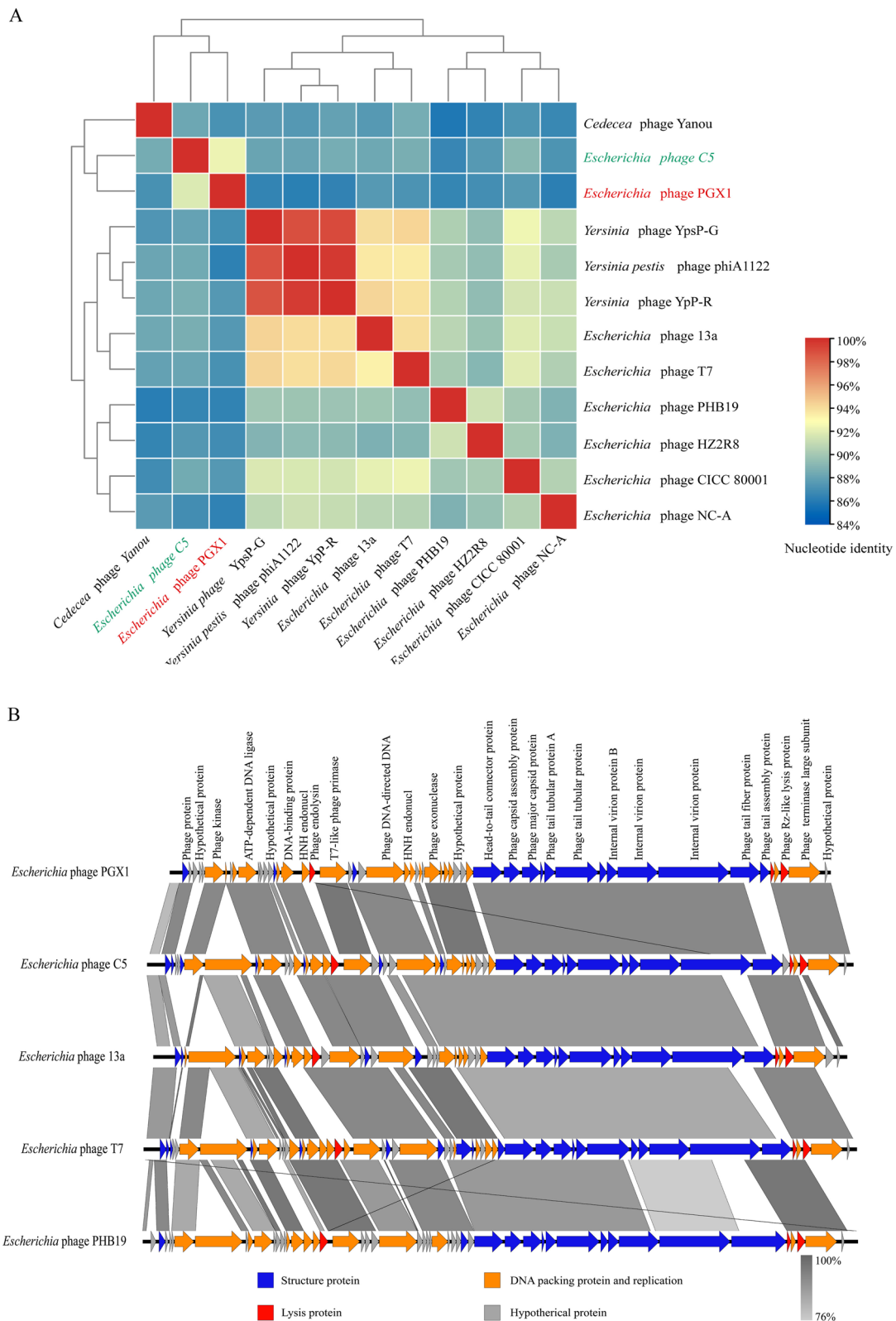
Furthermore, through phage genome bioinformatics analysis, it was discovered that phage PGX1 belongs to the family *Autographiviridae*, genus *Teseptimavirus*, shared more than 80% identity with other members of *Teseptimavirus*. The tail filament protein mainly acts as a receptor recognition protein binding to the host surface receptor protein (including lipopolysaccharide, fimbriae, outer membrane proteins, and flagella), thereby attaching the phage to the host surface (Simpson et al. 2016). The host range of a phage is determined by the specificity of its receptor. If receptor-binding proteins target multiple receptor proteins, the phage host range is broad; otherwise, the range is narrow (Nobrega et al. 2018). Because of this, phage PGX1, despite having a high degree of similarity with other phages, displayed an uneven host range. The reason behind the phage PGX1's ability to lyse O60 serotype *E. coli* strains is likewise related to the specificity of the tail filament protein. Therefore, we speculated that the O antigen might be the receptor of the phage PGX1, which needs to be further verified.

Furthermore, phages with a wide host range are more advantageous in treating multiple bacterial infections than those with a narrow host (Hyman 2019). However, the phage PGX1 only targeted multidrug-resistant *E. coli* of serotype O60. Besides, the results of the phage lysis curve showed that the phage could not completely kill the bacteria, and the phage-resistant mutants also emerged with the extension of time. Perhaps combining with other phages to form phage cocktails or with antibiotics to expand the target host range and delay the generation of resistant mutants may be better potential clinical application (Gao et al. 2022; Holger et al. 2022; Li et al. 2021; Wang et al. 2020).

The excellent stability of phages is important for long-term storage and clinical applications (Litt and Jaroni 2017). Studies have shown that changes in ambient temperature can affect phage morphology (Guglielmotti et al. 2011). High temperature can cause the degeneration of phage nucleic acids and proteins, leading to the disintegration of the phage structure (Jonczyk et al. 2011). Moreover, high concentrations of hydrogen and hydroxyl ions can cause the direct oxidation of the phage surface structure under extreme pH conditions, which results in structural dissociation and ultimately lead to phage mortality (Feng et al. 2003). The phage PGX1 showed excellent stability under different pH (pH4-10) and

(See figure on next page.)

Fig. 5 Homology similarity analysis between the genome-wide phage PGX1 and its homologous phages. **A** Heat map illustrating the phylogenetic relationship between phage PGX1 and eleven other homologous phages, based on ANI. The ANI values were calculated using the pairwise alignment coverage and percentage identity of Blastn, which ranged from 84 to 100%. The phage with the highest nucleotide identity value to PGX1 was identified in blue, while PGX1 itself was shown in red. **B** Comparison of whole genome linearization between phage PGX1 and homologous phages. The CDs are labeled with different colors: orange, blue, red and gray, respectively. Arrows indicate the direction of the CDs



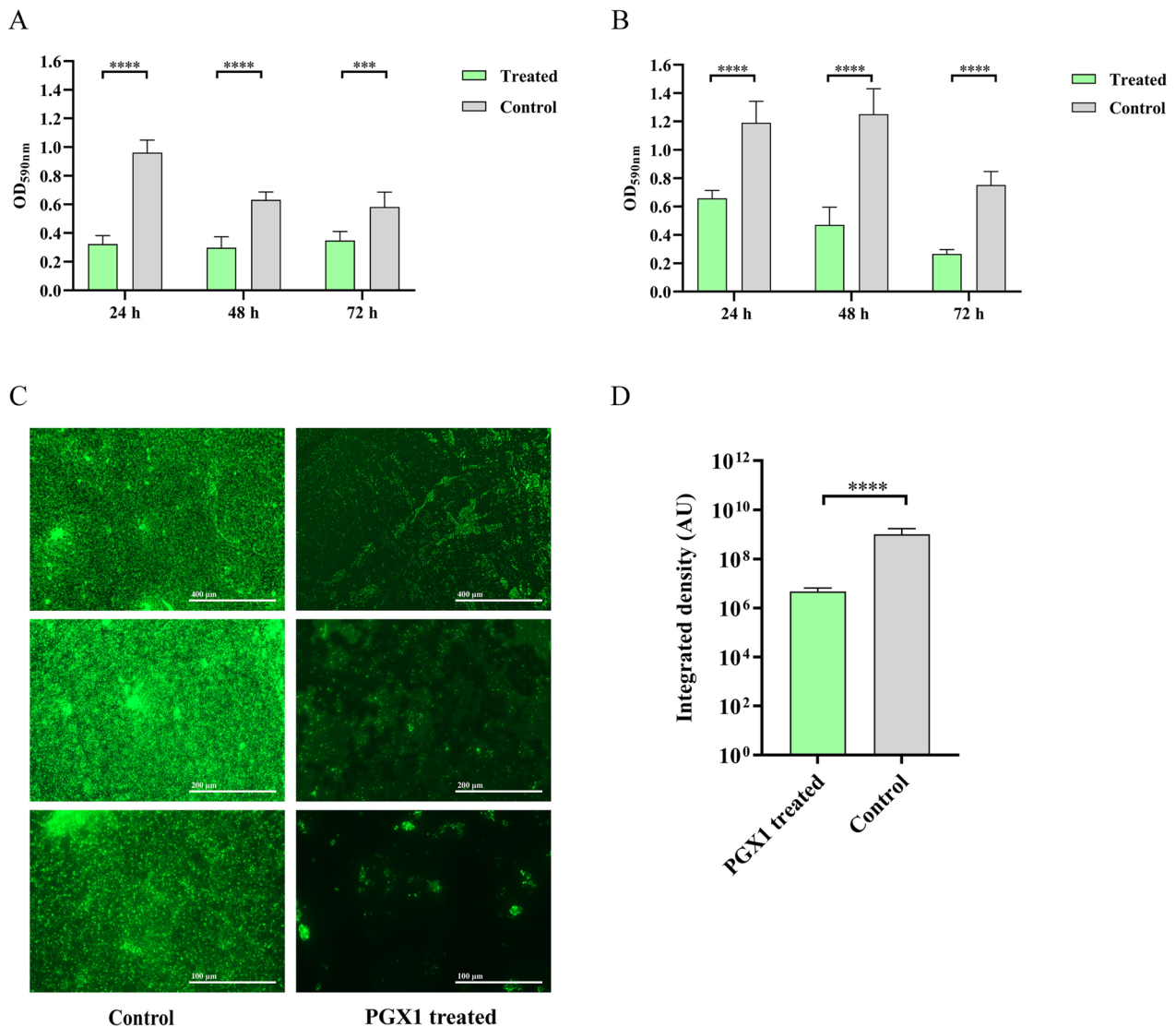


Fig. 6 In vitro efficiency of phage PGX1 in removing and inhibiting biofilm. **A** The efficiency of phage PGX1 removed biofilm. **B** The efficiency of phage PGX1 inhibited biofilm. **C** The biofilms were stained with the SYTOTM 9. The scale bars in the first row, the second row, and the third row represent 400, 200 and 100 μm , respectively. **D** The integrated density of fluorescence in EC6 biofilms was removed by phage PGX1. The statistical analysis was performed using the T-tests, and the difference was significant between the control group and the phage-treated group ($*** P \leq 0.001$)

temperature (4-40°C) conditions, which indicated that phage PGX1 could exist stably under a relatively wide range of environmental conditions and suggested its potential application in various environments.

The capacity of pathogens to develop biofilms on various substrates raises the risk of microbial cross-contamination, especially in the areas of food processing, healthcare facilities, and public health (Kim et al. 2022). Therefore, removing the pathogen biofilm remains a significant challenge. According to Jiang et al., the *E. coli* phage Flora was more effective in inhibiting multidrug-resistant *E. coli* biofilm formation than kanamycin sulfate in their study (Jiang et al. 2022). In our research, the

phage PGX1 was also discovered to have a considerable removing and inhibiting effect on the biofilm of multidrug-resistant ETEC. This finding further shows that phage PGX1 will be a useful antibiofilm strategy.

G. mellonella larvae are widely employed to assess the effectiveness of phages and various virulence tests because they have a similar immune system to vertebrates and a comprehensive evaluation system (Asai et al. 2023; Borman 2022; Feng et al. 2023; Kaczorowska et al. 2021; Li et al. 2023). Therefore, *G. mellonella* larvae were utilized as model organisms in this study to evaluate the control efficiency of the phage PGX1. Several studies have shown that high concentrations

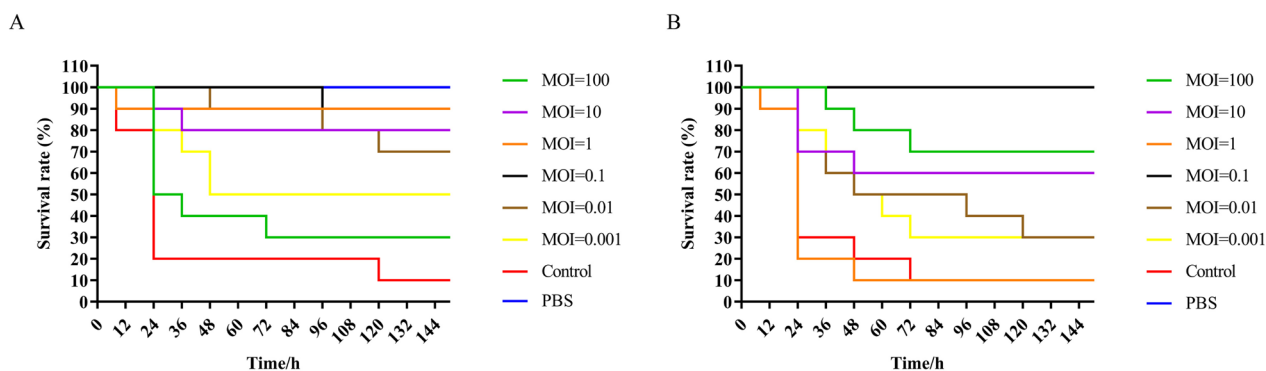


Fig. 7 The protective efficacy of phage PGX1 on *G. mellonella* larvae infected with *E. coli* EC6. **A** The survival rate of *G. mellonella* larvae inoculated with different MOI phage PGX1 to prevent EC6 infection. **B** The survival rate of the EC6-infected *G. mellonella* larvae treated with different MOI (multiplicity of infection)

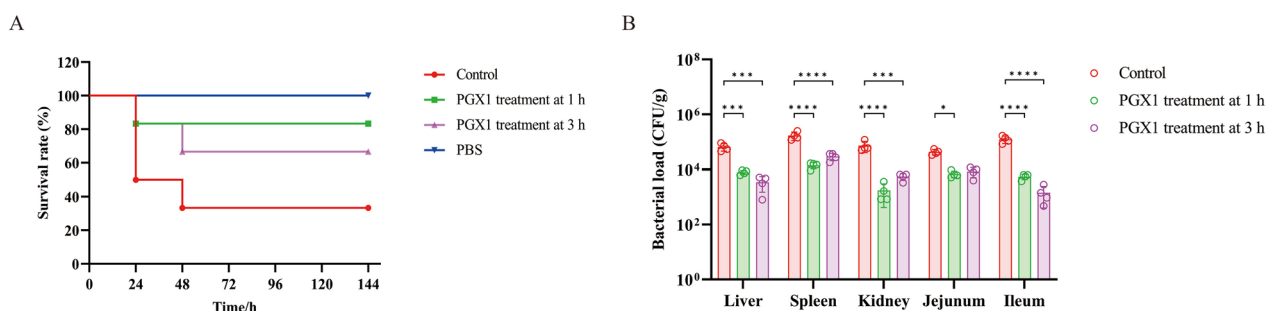


Fig. 8 The therapeutic efficacy of phage on mice infected with ETEC EC6. **A** The survival rate of mice treated with phage PGX1 at 1 and 3 h post-challenge. **B** Bacterial load in mice treated with phage PGX1 at 1 and 3 h after challenged by EC6. The EC6 bacterial load of the liver, spleen, kidney, jejunum and ileum of mice 48 h after phage PGX1 treatment. The statistical analysis was performed using the Two-way ANOVA. “*” “**” “***” and “****” represents $P < 0.05$, $P < 0.001$, and $P < 0.0001$, respectively

of phage in *G. mellonella* larvae may induce immune responses within the organism (Popescu et al. 2021; Wu et al. 2016; Wu and Yi 2016). Moreover, when the larvae were infected with bacteria after being injected with phage for a short period, the entry of bacteria further aggravated the immune response (Sheehan et al. 2021; Wu et al. 2014). At the same time, the phage lysed bacteria, leading to leakage of endotoxin and macromolecular proteins, further aggravated the immune response and caused an inflammatory storm (Wu et al. 2015a, 2015b), which explains the early-stage increased mortality of *G. mellonella* larvae when exposed to the phage at an MOI of 100. It was also the cause of the *G. mellonella* larvae’s poorer survival rate in the treatment trial at a high MOI (100 and 10) compared to an MOI of 0.1. However, when the time of bacterial infection was delayed, the high concentration of phage had a better defense effect against bacterial infection (Gorski et al. 2012; Van Belleghem et al. 2017).

On the other hand, the presence of high phage pressure would cause the production of anti-phage mutants

(Krut and Bekeredjian-Ding 2018; Oechslin 2018). Therefore, we hypothesized that the occurrence of anti-phage mutants may be responsible for the much worse therapeutic effect of high MOI (100 and 10) compared with low MOI (0.1 and 0.01) in the experiment of 3 h delayed therapy with phage. In their study, H.B. Erol et al. (Erol et al. 2022) reported that the phage Ec_P6 exhibited a high survival rate when used to treat *E. coli* infection in *G. mellonella* larvae at a low MOI of 0.01.

The efficacy of phage therapy was further assessed in an intraperitoneal infection-administration model in mice (Arumugam et al. 2022; Bao et al. 2020; Shi et al. 2021). The phage PGX1 treatment at an MOI of 0.1 improved the survival rate of mice infected with *E. coli* and significantly reduced the bacterial load in tissues and organs, indicating the potential clinical application of phage PGX1 in the control of multidrug-resistant *E. coli* infection. Although the experimental findings indicate that phage PGX1 is good in preventing and treating effects on multidrug-resistant ETEC EC6 infection, it is necessary to explore further and evaluate the influence of various

factors in the real environment before it can be used safely and effectively in clinical treatment.

Conclusion

We have discovered and characterized that the phage PGX1 exhibits a lytic effect on multidrug-resistant *E. coli* strains of serotype O60. Additionally, the phage PGX1 demonstrated effective inhibiting and removing effects on the biofilm formed by ETEC EC6, as well as preventive and therapeutic effects on infection with ETEC EC6 in the *G. mellonella* larvae and the mice. The study implied that phage PGX1 has the potential to control the disease caused by multidrug-resistant ETEC of serotype O60.

Materials and methods

Isolation and identification of bacteria

To isolate *E. coli* using MacConkey Agar medium (Qingdao Hope Bio-Technology Co., Ltd., Qingdao, China), we collected feces from piglets with diarrhea and intestinal contents from sick and deceased piglets from the pig farm in Guigang City. The isolated strains were amplified their 16S rRNA genes using universal primers [27F (5'-AGAGTTTGATCCTGGCTCAG-3') and 1492R (5'-GGTTACCTTGTACGACTT-3')], then sequenced by the company (BGI Genomics Co., Ltd., Shenzhen, China.). They were amplified using K88 (FaeG)-specific primers [F (5'-ATGAAAAGACTCTGATTGCACTG-3') and R (5'-GTAATAAGTAATTGCTACGTTTCAGCG-3')] to identify virulence factors of isolated *E. coli*. All sequences submitted to NCBI Blast for sequence alignment were identified at the genus level, and the isolated *E. coli* strains were named ECn (n stands for natural number). Based on CLSI standards, the drug sensitivity of the isolated *E. coli* was tested using the K-B method (CLSI, 2018.). Supplementary Table S2 contains a list of the strains used in this study. Other strains used are all maintained by the State Key Laboratory of Agricultural Microbiology, Huazhong Agricultural University.

Isolation and purification of the phage

E. coli phage was isolated and purified from sewage water in Guigang City using the double-layer plate method, with modifications as described previously (Xu et al. 2018). Briefly, the supernatant of sewage was mixed with EC6 culture (1:100, V/V) in the top medium (LB containing 0.75% (W/V) agar) and then plated on LA plates, incubated overnight at 37°C. A single plaque was added to the EC6 culture and incubated for 12 h at 37°C at 180 rpm after adding 5% (V/V) chloroform and centrifuged (10,000 g, 2 min). The supernatant was mixed with EC6 on the double-layer plates. Phage plaques were purified through three rounds of the above steps. Finally, the supernatant was filtered

using 0.22 µm filters (Millex-GP, USA) and centrifuged (110,000 g, 2.5 h, 4°C. The precipitations were resuspended in 2 mL SM buffer (10 mM MgSO₄, 50 mM Tris-HCl pH7.5, 100 mM NaCl, 5%) and further purified through the Cesium Chloride density gradient (Choi et al. 2020).

Transmission electron microscope (TEM)

The purified phage was applied to 200-mesh Formvar/carbon-supported copper grids (Beijing Zhongjingkeyi Technology Co., Ltd., Beijing, China) and stained with 2% (W/V) negative Phosphotungstic acid. Phage samples were captured under the transmission electron microscope (HITACHI H-7650, Japan) with an accelerating voltage of 100 kV.

Phage host range and efficiency of plating (EOP) determination

The host range and EOP of phage PGX1 were assessed by a spot test using 52 bacterial strains, including *E. coli* clinical strains, *E. coli* 15,857, BL21, B834, DH5α, *Salmonella enteritis*, *Pseudomonas aeruginosa*, *Klebsiella pneumoniae*, and so on, as previously described (Gao et al. 2023). Briefly, the phage PGX1 was subjected to a ten-fold serial dilution. Next, 10 µL of each diluted sample was spotted on double-layer agar plates, incubated at 37°C for 12 h. The EOP was calculated using the formula:

$$\text{The EOP} = (\text{PFU}_{\text{test strain}}) / (\text{PFU}_{\text{host strain EC6}}) \times 100\%$$

Determination of the optimal MOI and One-step growth curve assay

The optimal multiplicity of infection (MOI) was measured following previously established methods (Li et al. 2022) with some modifications. Logarithmic phase host bacteria EC6 were mixed with a filtered phage lysate at different MOI (100, 10, 1, 0.1, 0.01 and 0.001), incubated at 37°C with shaking at 180 rpm for 2 h, after centrifuged at 10,000 g for 2 min. Then, the supernatants of the mixture were subjected to a tenfold serial dilution, and phage titers were determined by spotting them in EC6-containing double-layer plates.

The one-step growth curve has been measured following a modified protocol (Gao et al. 2020). Briefly, the phage and EC6 culture were mixed at a MOI of 1, then incubated at 37°C, 180 rpm for 10 min. After centrifuging (10,000 g, 1 min), then the precipitation was collected and resuspended in a fresh medium, repeated twice. The mixtures were incubated at 37°C, 180 rpm. The culture was collected for centrifugation every 10 min beginning at 0 min. The collected supernatant was then serially diluted tenfold, followed by the determination of phage titer by spotting.

Generation of the phage lytic curve and bacterial growth rate

The phage lytic curves were generated by continuously monitoring the OD_{600nm} readings using the Bioscreen C system (Labsystems Oy, Helsinki, Finland) (Alexyuk et al. 2022). Briefly, in a 100-well microtiter plate, 200 µL of bacteria with an OD_{600nm} of 0.2 were added into each well. Subsequently, purified phage was added to different wells at various MOI (10, 1, 0.1 and 0.01). The mixtures were incubated at 37°C, 180 rpm, and OD_{600nm} readings were recorded every 0.5 h.

Analysis of thermal and pH stabilities

As described methods by Manohar et al., the phage PGX1 was exposed to different temperatures and pH levels to evaluate its activity (Manohar et al. 2018). Phage PGX1 were incubated at various temperatures (4°C, 12°C, 20°C, 30°C, 40°C, 50°C, 60°C, 70°C and 80°C) for 1 h. Phage PGX1 titer was then quantified by spot titer on double-layer agar plates with EC6 to assess its thermostability. The purified phage (100 µL) was combined with SM buffer (900 µL) at various pH levels (pH2-12), then incubated at 37°C for 1 h, followed by testing the phage titer.

DNA extraction and genome sequence analysis

DNase I and RNase A (Vazyme, Nanjing Vazyme Biotech Co., Ltd., Nanjing, China) were added to the sample to remove any contamination of host nucleotides at a final concentration of 1 µg/mL. The genomic DNA of the phage was extracted using the viral genome extraction kit (Omega Bio-Tek Inc., Doraville, GA, United States). Then, the phage genomes were sequenced using the Illumina MiSeq system (300-bp paired reads, San Diego, CA, USA) at Novogene Bioinformatics Technology Co. Ltd. (Beijing, China) and assembled in SPAdes V. 3.15.2 (Prjibelski et al. 2020).

The assembled genome sequence was subjected to alignment and annotation using the BLASTp (<https://blast.ncbi.nlm.nih.gov/Blast.cgi>) and RAST (<https://rast.nmpdr.org/>) tools (Overbeek et al. 2014). Then, the phage genome was constructed as a circle map using the online software Proksee (<https://proksee.ca/>) (Grant et al. 2023). The putative tRNA-encoding genes, virulence signatures, and antibiotic resistance genes in the phage genome were determined using the tRNAscan-SE platform (<http://lowelab.ucsc.edu/tRNAscan-SE/>), the Virulence Factor Database (VFDB, <http://www.mgc.ac.cn/cgi-bin/VFs/v5/main.cgi>) and the Comprehensive Antibiotic Resistance Database (CARD, <https://card.mcmaster.ca/analyze/blast>), respectively (Alcock et al. 2020; Liu et al. 2022; Lowe and Chan 2016).

According to the ICTV classification reports, the amino acid sequences of terminase large subunits from different phages were downloaded from NCBI databases. Phylogenetic analysis was constructed using MEGA 7 software, employing the neighbor-joining method with 1,000 bootstrap replicates. To further compare the similarity of phage whole genomes, the whole genome of phage PGX1 was subjected to BLASTn, and the resulting Average Nucleotide Identity (ANI) values were calculated using the online analysis site JSpeciesWS (<https://jspecies.ribohost.com/jspeciesws/#home>). Evolutionary relationship analysis was then conducted using TB tools (Chen et al. 2020; Richter et al. 2016). Phages with high homology to PGX1 were selected, and their genomes were compared by Easyfig V. 2.2.5 software (Sullivan et al. 2011).

In vitro biofilm development model

The effect of phage PGX1 on biofilm was evaluated using the microtiter plate assay, as previously described (Duarte et al. 2021), with some modifications. To assess the efficacy of phage PGX1 to remove biofilm, log-phase *E. coli* EC6 and LB medium (Oxoid, Basingstoke, UK) (1:100, V/V) were mixed into a 96-well plate, incubated at 37°C for 48 h to form a biofilm, then washed three times with 10 mM PBS (pH7.4). The phage and LB medium (1:1, V/V) were added to the plates and incubated at 37°C for 24, 48 and 72 h, respectively. Then, the plates were washed three times with 10 mM PBS, dried, and fixed at a high temperature. Each well was stained with 1% crystal violet solution and incubated at 37°C for 2 h, washed excess dye, and dried. Next, the precipitate was dissolved by 200 µL of 33% glacial acetic acid and measured the absorbance of OD_{590nm}. Meanwhile, the biofilms formed on cell slides in 24-well plates were washed three times with 10 mM PBS after being treated with PGX1 for 24 h and stained with the SYTO™ 9 dye (MKBio, Shanghai MKBio Technology Co., Ltd., Shanghai, China), then observed under an inverted fluorescence microscope to capture images. The integrated density of fluorescence of the biofilm was then analyzed using ImageJ (Gonzalez et al. 2017; Peeters et al. 2008).

To determine the inhibition of biofilm growth by phage PGX1, phage PGX1 and LB medium (1:1, V/V) were added in a 96-well plate, while log phase bacterial EC6 was added at 1:100, incubated at 37°C for 24, 48 and 72 h, respectively. Then, the absorbance of OD_{590nm} was measured according to the method described above.

In vivo investigation on the *G. mellonella* larvae

The *G. mellonella* larvae with a length of 2–3 cm and no discoloration were selected as the model organisms to evaluate the potential effectiveness of phage against multidrug-resistant ETEC EC6 (Antoine et al. 2021; Feng et al. 2023). They were removed from the refrigerator at 4°C and reactivated at room temperature for 2 h. To assess the LD₅₀ of EC6, PBS and various concentrations of *E. coli* EC6 were injected into *G. mellonella* larvae (25 µL/per, 10/group) using a 1 mL insulin needle (Yiguang, Shandong Yiguang Medica Instrument Co., Ltd., Shandong, China). The infected *G. mellonella* larvae were kept in incubation at 37°C and monitored daily for larval mortality for 7 d. Three independent replicates of the experiment were performed for each group of infections.

Different MOI of phage PGX1 suspensions (25 µL) were injected into the larvae at 1 h and 3 h prior to infection to evaluate the protective effect of phage PGX1 on *G. mellonella* larvae infected with EC6. Then, the larvae were challenged to the LD₅₀ of EC6 and incubated at 37°C for 7 d to monitor larval mortality. The *G. mellonella* larvae were first challenged to 1 LD₅₀ of EC6 to explore the therapeutic efficacy of phage PGX1 on the *G. mellonella* larvae infected with EC6. The *G. mellonella* larvae were then injected with phage PGX1 (25 µL) at different MOI at 1 h and 3 h post-infection. Subsequently, they were then incubated at 37°C and monitored for 7 d to assess larval mortality of the larvae as a measure of the therapeutic effect of phage PGX1 on the *G. mellonella* larvae infected with EC6. These experiments were performed in triplicate to ensure statistical robustness and reproducibility. Prevention and treatment trials were categorized into eight distinct groups:

- Group 1: PBS + PBS (Healthy Control),
- Group 2: PBS + *E. coli* EC6 (10⁵ CFU) / *E. coli* EC6 (10⁵ CFU) + PBS (Infection Control),
- Group 3: phage PGX1 (100 MOI) + *E. coli* EC6 (10⁵ CFU),
- Group 4: phage PGX1 (10 MOI) + *E. coli* EC6 (10⁵ CFU),
- Group 5: phage PGX1 (1 MOI) + *E. coli* EC6 (10⁵ CFU),
- Group 6: phage PGX1 (0.1 MOI) + *E. coli* EC6 (10⁵ CFU),
- Group 7: phage PGX1 (0.01 MOI) + *E. coli* EC6 (10⁵ CFU),
- Group 8: phage PGX1 (0.001 MOI) + *E. coli* EC6 (10⁵ CFU).

In vivo infection model in mice

The six-week-old female specific-pathogen-free (SPF) BALB/c mice were divided into 4 groups (10/group): (i) PBS negative control group, (ii) *E. coli* EC6 challenge group, (iii) phage PGX1 treatment at 1 h after challenge, (iv) phage PGX1 treatment at 3 h after challenge. The mice were challenged with EC6 (5 × 10⁸ CFU/per, 150 µL) by intraperitoneal injection (i.p.), and the mice in the negative control group were injected with an equivalent volume 10 mM PBS (pH 7.4). Then, the therapeutic groups were injected with 150 µL phage PGX1 at MOI of 0.1 (5 × 10⁷ PFU/per) at 1 and 3 h post-challenge, respectively. The survival rate and physiological state of the mice were monitored for 7 d. In addition, four mice were randomly selected to measure bacterial load in their tissues and organs after 48 h. Briefly, the liver, spleen, kidney, jejunum, and ileum of the mice were collected, weighed, and added to 1 mL of 10 mM PBS (pH 7.4) for homogenizing. The tissue homogenates were diluted in a ten-fold gradient, and 100 µL of each diluent solution was plated on the LA plates containing 50 µg/mL chloramphenicol. The plates were incubated at 37°C for 12 h before colony counting.

All animal experiments were performed with the approval of the Scientific Ethic Committee of Huazhong Agricultural University (ID Number: HZAUMO-2023–0335).

Statistical analysis

All experiments were performed in triplicate, and the data were presented as means ± SD. Statistical analysis and comparisons were conducted using GraphPad Prism 9.5 software (GraphPad Software, San Diego, CA, USA) via T-tests and Two-way ANOVA.

Supplementary Information

The online version contains supplementary material available at <https://doi.org/10.1186/s44149-024-00112-3>.

Additional file 1: Supplementary Fig. S1. Detection and homology analysis of the hair specificity of clinical isolates of multidrug-resistant *E. coli* FaeG (K88). (A) Identification of FaeG-specific fragments by PCR amplification using FaeG-specific primers. (B) Sequencing results of the corresponding base sequence of the FaeG-specific primer amplified fragment of *E. coli* EC6. (C) The amino acids sequence (14–275) differences between the FaeG fragment of the isolated strains and its Blastn homologous sequence *E. coli* SEC799 FaeG gene (GenBank: DQ307494). **Supplementary Fig. S2.** Evaluating the protection and therapeutic effect of phage PGX1 against *G. mellonella* larvae infected with ETEC EC6. (A) The LD₅₀ of *E. coli* EC6 to *G. mellonella* larvae. Doses 1 to 8 represented EC6 infection doses of 2 × 10⁷ CFU, 1 × 10⁷ CFU, 2 × 10⁶ CFU, 1 × 10⁶ CFU, 2 × 10⁵ CFU, 1 × 10⁵ CFU, 2 × 10⁴ CFU, and 1 × 10⁴ CFU, respectively. (B) Safety evaluation of different titers of phage PGX1 injected into *G. mellonella* larvae. Dose 1 to 6 represented phage PGX1 injection dose: 5 × 10⁷ PFU, 5 × 10⁶ PFU, 5 × 10⁵ PFU, 5 × 10⁴ PFU, 5 × 10³ PFU, and 5 × 10² PFU, respectively. (C) Protective effect of phage PGX1 in *G. mellonella* larvae against EC6 challenge after 3 h. (D) The therapeutic effect of phage PGX1 on EC6-infected *G. mellonella* larvae for 3 h. **Table S1.** Antibiotic resistance profile of *E. coli* isolations in this study. **Table S2.** Lytic profile of phage PGX1. **Table S3.** Predicted ORFs of the PGX1.

Acknowledgements

Thank Jianbo Cao and Limin He (National Key Laboratory of Agricultural Microbiology, Huazhong Agricultural University) for their support of TEM.

Authors' contributions

DYH: Conceptualization, Methodology, Visualization, Writing original draft, Writing review & editing. PQ: Conceptualization, supervision, Funding acquisition, Project administration. DYG: Methodology, Software, Visualization, XML: Writing review & editing. HYJ, LKW, and SW: Software. XML: Conceptualization, Project administration, Supervision. All authors have read and approved the final manuscript.

Funding

This work was supported by grants from the National Program on Key Research Project of China [2022YFD1800800, 2021YFD1800300] and the Yingzi Tech & Huazhong Agricultural University Intelligent Research Institute of Food Health [No. IRIFH202209, No. IRIFH202301]. The National Program on Key Research Project of China, 2022YFD1800800, Ping Qian, 2021YFD1800300, Ping Qian, The Yingzi Tech & Huazhong Agricultural University Intelligent Research Institute of Food Health, IRIFH202209, Ping Qian, IRIFH202301, Ping Qian

Availability of data and materials

The GenBank accession number of phage complete genome are OQ703770 (*Escherichia* phage PGX1), NC_011045.1 (*Escherichia* phage 13a), NC_048079.1 (*Escherichia* phage C5), MN481365.1 (*Escherichia* phage vB_EcoP_PHB19), NC_001604.1 (*Escherichia* phage T7), ON568193.1 (*Cedecea* phage Yanou), NC_027387.1 (*Escherichia* phage CICC 80001), NC_047923.1 (*Escherichia* phage HZ2R8), MK310182.1 (*Escherichia* phage NC-A), NC_004777.1 (*Yersinia pestis* phage phiA1122), JQ965701.1 (*Yersinia* phage YpP-R), NC_047940.1 (*Yersinia* phage YpsP-G).

Declarations

Competing interests

The authors declare no conflict of interest.

Received: 27 September 2023 Accepted: 26 January 2024

Published online: 13 March 2024

References

- Abri, R., A. Javadi, R. Asghari, V. Razavilar, T.Z. Salehi, F. Safaeeyan, and M.A. Rezaee. 2019. Surveillance for enterotoxigenic & enteropathogenic *Escherichia coli* isolates from animal source foods in Northwest Iran. *Indian Journal of Medical Research* 150: 87–91. https://doi.org/10.4103/ijmr.IJMR_2019_17.
- Alcock, B.P., A.R. Raphenya, T.T.Y. Lau, K.K. Tsang, M. Bouchard, A. Edalatmand, W. Huynh, A.V. Nguyen, A.A. Cheng, S. Liu, et al. 2020. CARD 2020: Antibiotic resistome surveillance with the comprehensive antibiotic resistance database. *Nucleic Acids Research* 48: D517–D525. <https://doi.org/10.1093/nar/gkz935>.
- Alexyuk, P., Bogoyavlenskij, A., Alexyuk, M., Akanova, K., Moldakhanov, Y., and V. Berezin. 2022. Isolation and characterization of lytic bacteriophages active against clinical strains of *E. coli* and development of a phage antimicrobial cocktail. *Viruses* 14. <https://doi.org/10.3390/v14112381>.
- Alsaadi, A., B. Beamud, M. Easwaran, F. Abdelrahman, A. El-Shibiny, M.F. Algoribi, and P. Domingo-Calap. 2021. Learning from mistakes: the role of phages in pandemics. *Frontiers in Microbiology* 12: 653107. <https://doi.org/10.3389/fmicb.2021.653107>.
- Antimicrobial Resistance, C. 2022. Global burden of bacterial antimicrobial resistance in 2019: a systematic analysis. *Lancet* 399: 629–655. [https://doi.org/10.1016/s0140-6736\(21\)02724-0](https://doi.org/10.1016/s0140-6736(21)02724-0).
- Antoine, C., Laforet, F., Blasdel, B., Fall, A., Duprez, J.N., Mainil, J., Delcenserie, V., and D. Thiry. 2021. In vitro characterization and in vivo efficacy assessment in galleria mellonella larvae of newly isolated bacteriophages against *Escherichia coli* K1. *Viruses-Basel* 13. <https://doi.org/10.3390/v13102005>.
- Arumugam, S.N., P. Manohar, S. Sukumaran, S. Sadagopan, B. Loh, S. Leptihn, and R. Nachimuthu. 2022. Antibacterial efficacy of lytic phages against multidrug-resistant *Pseudomonas aeruginosa* infections in bacteremia mice models. *BMC Microbiology* 22: 187. <https://doi.org/10.1186/s12866-022-02603-0>.
- Asai, M., Li, Y., Newton, S.M., Robertson, B.D., and Langford, P.R. 2023. Galleria mellonella-intracellular bacteria pathogen infection models: the ins and outs. *FEMS Microbiol Rev* 47. <https://doi.org/10.1093/femsre/fuad011>.
- Bao, H., Y. Zhou, K. Shahin, H. Zhang, F. Cao, M. Pang, X. Zhang, S. Zhu, A. Olaniran, S. Schmidt, and R. Wang. 2020. The complete genome of lytic Salmonella phage vB_SenM-PA13076 and therapeutic potency in the treatment of lethal Salmonella Enteritidis infections in mice. *Microbiological Research* 237: 126471. <https://doi.org/10.1016/j.micres.2020.126471>.
- Borman, A.M. 2022. The use of galleria mellonella larvae to study the pathogenicity and clonal lineage-specific behaviors of the emerging fungal pathogen candida auris. *Methods in Molecular Biology* 2517: 287–298. https://doi.org/10.1007/978-1-0716-2417-3_23.
- Bowler, P.G. 2018. Antibiotic resistance and biofilm tolerance: a combined threat in the treatment of chronic infections. *Journal of Wound Care* 27: 273–277. <https://doi.org/10.12968/jowc.2018.27.5.273>.
- Chan, H.K., and R.Y.K. Chang. 2022. Inhaled delivery of anti-pseudomonal phages to tackle respiratory infections caused by superbugs. *Journal of Aerosol Medicine and Pulmonary Drug Delivery* 35: 73–82. <https://doi.org/10.1089/jamp.2021.0045>.
- Chaudhary, N., B. Mohan, R.S. Mavuduru, Y. Kumar, and N. Taneja. 2022. Characterization, genome analysis and in vitro activity of a novel phage vB_EcoA_RDN8.1 active against multi-drug resistant and extensively drug-resistant biofilm-forming uropathogenic *Escherichia coli* isolates, India. *Journal of Applied Microbiology* 132: 3387–3404. <https://doi.org/10.1111/jam.15439>.
- Chen, C., H. Chen, Y. Zhang, H.R. Thomas, M.H. Frank, Y. He, and R. Xia. 2020. TBtools: an integrative toolkit developed for interactive analyses of big biological data. *Molecular Plant* 13: 1194–1202. <https://doi.org/10.1016/j.molp.2020.06.009>.
- Choi, I.Y., D.H. Park, B.A. Chin, C. Lee, J. Lee, and M.K. Park. 2020. Exploring the feasibility of *Salmonella Typhimurium*-specific phage as a novel bio-receptor. *Journal of Animal Science and Technology* 62: 668–681. <https://doi.org/10.5187/jast.2020.62.5.668>.
- CLSI. 2018. *Performance standards for antimicrobial disk susceptibility test, M02*, 13th ed., 92. Wayne: Clinical and Laboratory Standards Institute.
- Dion, M.B., F. Oechslin, and S. Moineau. 2020. Phage diversity, genomics and phylogeny. *Nature Reviews Microbiology* 18: 125–138. <https://doi.org/10.1038/s41579-019-0311-5>.
- Duarte, A.C., L. Fernandez, V. De Maesschalck, D. Gutierrez, A.B. Campelo, Y. Briers, R. Lavigne, A. Rodriguez, and P. Garcia. 2021. Synergistic action of phage phiPLA-RODI and lytic protein CHAPSH3b: A combination strategy to target *Staphylococcus aureus* biofilms. *NPJ Biofilms and Microbiomes* 7: 39. <https://doi.org/10.1038/s41522-021-00208-5>.
- El-Shibiny, A., S. El-Sahhar, and M. Adel. 2017. Phage applications for improving food safety and infection control in Egypt. *Journal of Applied Microbiology* 123: 556–567. <https://doi.org/10.1111/jam.13500>.
- Erol, H.B., B. Kaskatepe, S. Ozturk, and Z. Safi Oz. 2022. The comparison of lytic activity of isolated phage and commercial Intesti bacteriophage on ESBL producer *E coli* and determination of Ec_P6 phage efficacy with in vivo *Galleria mellonella* larvae model. *Microbial Pathogenesis* 167: 105563. <https://doi.org/10.1016/j.micpath.2022.105563>.
- Feng, Y.Y., S.L. Ong, J.Y. Hu, X.L. Tan, and W.J. Ng. 2003. Effects of pH and temperature on the survival of coliphages MS2 and Qbeta. *Journal of Industrial Microbiology and Biotechnology* 30: 549–552. <https://doi.org/10.1007/s10295-003-0080-y>.
- Feng, J., F. Li, L. Sun, L. Dong, L. Gao, H. Wang, L. Yan, and C. Wu. 2023. Characterization and genome analysis of phage vB_KpnS_SXFY507 against *Klebsiella pneumoniae* and efficacy assessment in *Galleria mellonella* larvae. *Frontiers in Microbiology* 14: 1081715. <https://doi.org/10.3389/fmicb.2023.1081715>.
- Gao, M., C. Wang, X. Qiang, H. Liu, P. Li, G. Pei, X. Zhang, Z. Mi, Y. Huang, Y. Tong, and C. Bai. 2020. Isolation and characterization of a novel bacteriophage infecting carbapenem-resistant *klebsiella pneumoniae*. *Current Microbiology* 77: 722–729. <https://doi.org/10.1007/s00284-019-01849-8>.
- Gao, D., H. Ji, L. Wang, X. Li, D. Hu, J. Zhao, S. Wang, P. Tao, X. Li, and P. Qian. 2022. Fitness trade-offs in phage cocktail-resistant salmonella enterica serovar enteritidis results in increased antibiotic susceptibility and reduced

- virulence. *Microbiology Spectrum* 10: e0291422. <https://doi.org/10.1128/spectrum.02914-22>.
- Gao, D., H. Ji, X. Li, X. Ke, X. Li, P. Chen, and P. Qian. 2023. Host receptor identification of a polyvalent lytic phage GSP044, and preliminary assessment of its efficacy in the clearance of *Salmonella*. *Microbiological Research* 273: 127412. <https://doi.org/10.1016/j.micres.2023.127412>.
- Gonzalez, S., Fernandez, L., Campelo, A.B., Gutierrez, D., Martinez, B., Rodriguez, A., and Garcia, P., 2017. The behavior of staphylococcus aureus dual-species biofilms treated with bacteriophage phiPLA-RODI depends on the accompanying microorganism. *Applied and Environmental Microbiology* 83. <https://doi.org/10.1128/AEM.02821-16>.
- Goodarzi, F., M. Hallajzadeh, M. Sholeh, M. Talebi, V.P. Mahabadi, and N. Amir-mozafari. 2021. Biological characteristics and anti-biofilm activity of a lytic phage against vancomycin-resistant *Enterococcus faecium*. *Iranian Journal of Microbiology* 13: 691–702. <https://doi.org/10.18502/ijm.v13i5.7436>.
- Gordillo Altamirano, F.L., and J.J. Barr. 2019. Phage therapy in the postantibiotic era. *Clinical Microbiology Reviews* 32. <https://doi.org/10.1128/CMR.00066-18>.
- Gorski, A., R. Miedzybrodzki, J. Borysowski, K. Dabrowska, P. Wierzbicki, M. Ohams, G. Korczak-Kowalska, N. Olszowska-Zaremba, M. Lusiak-Szelachowska, M. Klak, et al. 2012. Phage as a modulator of immune responses: practical implications for phage therapy. *Advances in Virus Research* 83: 41–71. <https://doi.org/10.1016/B978-0-12-394438-2.00002-5>.
- Grant, J.R., E. Enns, E. Marinier, A. Mandal, E.K. Herman, C.Y. Chen, M. Graham, G. Van Domselaar, and P. Stothard. 2023. Proksee: In-depth characterization and visualization of bacterial genomes. *Nucleic Acids Research*. <https://doi.org/10.1093/nar/gkac326>.
- Gresse, R., F. Chaucheyras-Durand, M.A. Fleury, T. Van de Wiele, E. Forano, and S. Blanquet-Diot. 2017. Gut microbiota dysbiosis in postweaning piglets: understanding the keys to health. *Trends in Microbiology* 25: 851–873. <https://doi.org/10.1016/j.tim.2017.05.004>.
- Guglielmotti, D.M., D.J. Mercanti, J.A. Reinheimer, and L. Quiberoni Adel. 2011. Review: Efficiency of physical and chemical treatments on the inactivation of dairy bacteriophages. *Frontiers in Microbiology* 2: 282. <https://doi.org/10.3389/fmicb.2011.00282>.
- Harms, A., Maisonneuve, E., and Gerdes, K., 2016. Mechanisms of bacterial persistence during stress and antibiotic exposure. *Science* 354. <https://doi.org/10.1126/science.aaf4268>.
- Hathroubi, S., M.A. Mekni, P. Domenico, D. Nguyen, and M. Jacques. 2017. Biofilms: microbial shelters against antibiotics. *Microbial Drug Resistance* 23: 147–156. <https://doi.org/10.1089/mdr.2016.0087>.
- Holger, D.J., K.L. Lev, R. Kebriaei, T. Morrisette, R. Shah, J. Alexander, S.M. Lehman, and M.J. Rybak. 2022. Bacteriophage-antibiotic combination therapy for multidrug-resistant *Pseudomonas aeruginosa*: In vitro synergy testing. *Journal of Applied Microbiology* 133: 1636–1649. <https://doi.org/10.1111/jam.15647>.
- Hosangadi, D., P.G. Smith, D.C. Kaslow, B.K. Giersing, E. Who, Shigella Vaccine Consultation Expert, G. 2019. WHO consultation on ETEC and Shigella burden of disease, Geneva, 6–7th April 2017: meeting report. *Vaccine* 37: 7381–7390. <https://doi.org/10.1016/j.vaccine.2017.10.011>.
- Hyman, P., 2019. Phages for phage therapy: isolation, characterization, and host range breadth. *Pharmaceuticals (Basel)* 12. <https://doi.org/10.3390/ph12010035>.
- Jiang, L., Y. Jiang, W. Liu, R. Zheng, and C. Li. 2022. Characterization of the Lytic phage flora with a broad host range against multidrug-resistant *Escherichia coli* and evaluation of its efficacy against *E. coli* biofilm formation. *Frontiers in Veterinary Science* 9: 906973. <https://doi.org/10.3389/fvets.2022.906973>.
- Jonczyk, E., M. Klak, R. Miedzybrodzki, and A. Gorski. 2011. The influence of external factors on bacteriophages—review. *Folia Microbiologica (Praha)* 56: 191–200. <https://doi.org/10.1007/s12223-011-0039-8>.
- Kaczorowska, J., Casey, E., Lugli, G.A., Ventura, M., Clarke, D.J., van Sinderen, D., and J. Mahony. 2021. In vitro and in vivo assessment of the potential of *Escherichia coli* phages to treat infections and survive gastric conditions. *Microorganisms* 9. <https://doi.org/10.3390/microorganisms9091869>.
- Kim, U., J.H. Kim, and S.W. Oh. 2022. Review of multi-species biofilm formation from foodborne pathogens: Multi-species biofilms and removal methodology. *Critical Reviews in Food Science and Nutrition* 62: 5783–5793. <https://doi.org/10.1080/10408398.2021.1892585>.
- Krut, O., and I. Bekeredjian-Ding. 2018. Contribution of the immune response to phage therapy. *The Journal of Immunology* 200: 3037–3044. <https://doi.org/10.4049/jimmunol.1701745>.
- Levin-Reisman, I., I. Ronin, O. Gefen, I. Braniss, N. Shosh, and N.Q. Balaban. 2017. Antibiotic tolerance facilitates the evolution of resistance. *Science* 355: 826–830. <https://doi.org/10.1126/science.aaj2191>.
- Lewis, K. 2020. The science of antibiotic discovery. *Cell* 181: 29–45. <https://doi.org/10.1016/j.cell.2020.02.056>.
- Li, X., Y. He, Z. Wang, J. Wei, T. Hu, J. Si, G. Tao, L. Zhang, L. Xie, A.E. Abdalla, et al. 2021. A combination therapy of Phages and Antibiotics: Two is better than one. *International Journal of Biological Sciences* 17: 3573–3582. <https://doi.org/10.7150/ijbs.60551>.
- Li, F., L. Li, Y. Zhang, S. Bai, L. Sun, J. Guan, W. Zhang, X. Cui, J. Feng, and Y. Tong. 2022. Isolation and characterization of the novel bacteriophage vB_SmaS_BUCT626 against *Stenotrophomonas maltophilia*. *Virus Genes* 58: 458–466. <https://doi.org/10.1007/s11262-022-01917-5>.
- Li, Y., M. Pu, P. Han, M. Li, X. An, L. Song, H. Fan, Z. Chen, and Y. Tong. 2023. Efficacy in Galleria mellonella larvae and application potential assessment of a new bacteriophage BUCT700 extensively lyse *Stenotrophomonas maltophilia*. *Microbiology Spectrum* 11: e0403022. <https://doi.org/10.1128/spectrum.04030-22>.
- Litt, P.K., and D. Jaroni. 2017. Isolation and physiomorphological characterization of *Escherichia coli* O157:H7-infecting bacteriophages recovered from beef cattle operations. *International Journal of Microbiology* 2017: 7013236. <https://doi.org/10.1155/2017/7013236>.
- Liu, B., D. Zheng, S. Zhou, L. Chen, and J. Yang. 2022. VFDB 2022: A general classification scheme for bacterial virulence factors. *Nucleic Acids Research* 50: D912–D917. <https://doi.org/10.1093/nar/gkac1107>.
- Lowe, T.M., and P.P. Chan. 2016. tRNAscan-SE On-line: Integrating search and context for analysis of transfer RNA genes. *Nucleic Acids Research* 44: W54–57. <https://doi.org/10.1093/nar/gkw413>.
- Lu, T., Moxley, R.A., and W. Zhang. 2019. Mapping the neutralizing epitopes of enterotoxigenic *Escherichia coli* K88 (F4) fimbrial adhesin and major subunit FaeG. *Applied and Environmental Microbiology* 85. <https://doi.org/10.1128/aem.00329-19>.
- Manohar, P., A.J. Tamhankar, C.S. Lundborg, and N. Ramesh. 2018. Isolation, characterization and in vivo efficacy of *Escherichia coli* phage myPSH1131. *PLoS One* 13: e0206278. <https://doi.org/10.1371/journal.pone.0206278>.
- McDougall, D.L., C.D. Soutar, B.J. Perry, C. Brown, D. Alexander, C.K. Yost, and J. Starvinides. 2020. Isolation and characterization of vB_PagP-SK1, a T7-Like phage infecting *Pantoea agglomerans*. *Phage (new Rochelle)* 1: 45–56. <https://doi.org/10.1089/phage.2019.0012>.
- Moghadam, M.T., N. Amirmozafari, A. Shariati, M. Hallajzadeh, S. Mirkalantari, A. Khoshbayan, and F.M. Jazi. 2020. How phages overcome the challenges of drug resistant bacteria in clinical infections. *Infection and Drug Resistance* 13: 45–61. <https://doi.org/10.2147/ldr.S234353>.
- Mohammadi, M., M. Saffari, and S.D. Siadat. 2023. Phage therapy of antibiotic-resistant strains of *Klebsiella pneumoniae*, opportunities and challenges from the past to the future. *Folia Microbiologica (Praha)* 68: 357–368. <https://doi.org/10.1007/s12223-023-01046-y>.
- Nobrega, F.L., M. Vlot, P.A. de Jonge, L.L. Dreesens, H.J.E. Beaumont, R. Lavigne, B.E. Dutilh, and S.J.J. Brouns. 2018. Targeting mechanisms of tailed bacteriophages. *Nature Reviews Microbiology* 16 (12): 760–773. <https://doi.org/10.1038/s41579-018-0070-8>.
- Oechslin, F., 2018. Resistance development to bacteriophages occurring during bacteriophage therapy. *Viruses* 10. <https://doi.org/10.3390/v10070351>.
- Ooi, M.L., A.J. Drilling, S. Morales, S. Fong, S. Moraitis, L. Macias-Valle, S. Vreugde, A.J. Psaltis, and P.J. Wormald. 2019. Safety and tolerability of bacteriophage therapy for chronic rhinosinusitis due to *Staphylococcus aureus*. *Jama Otolaryngology* 145: 723–729. <https://doi.org/10.1001/jamaoto.2019.1191>.
- Overbeek, R., R. Olson, G.D. Pusch, G.J. Olsen, J.J. Davis, T. Disz, R.A. Edwards, S. Gerdes, B. Parrello, M. Shukla, et al. 2014. The SEED and the rapid annotation of microbial genomes using Subsystems Technology (RAST). *Nucleic Acids Research* 42: D206–214. <https://doi.org/10.1093/nar/gkt1226>.
- Peeters, E., H.J. Nelis, and T. Coenye. 2008. Comparison of multiple methods for quantification of microbial biofilms grown in microtiter plates. *Journal of Microbiological Methods* 72: 157–165. <https://doi.org/10.1016/j.jmimet.2007.11.010>.
- Popescu, M., J.D. Van Belleghem, A. Khosravi, and P.L. Bollyky. 2021. Bacteriophages and the immune system. *Annual Review of Virology* 8: 415–435. <https://doi.org/10.1146/annurev-virology-091919-074551>.

- Prazak, J., L.G. Valente, M. Iten, L. Federer, D. Grandgirard, S. Soto, G. Resch, S.L. Leib, S.M. Jakob, M. Haenggi, et al. 2022. Benefits of aerosolized phages for the treatment of pneumonia due to methicillin-resistant *Staphylococcus aureus*: an experimental study in rats. *Journal of Infectious Diseases* 225: 1452–1459. <https://doi.org/10.1093/infdis/jiab112>.
- Prijbelski, A., D. Antipov, D. Meleshko, A. Lapidus, and A. Korobeynikov. 2020. Using spades de novo assembler. *Current Protocols in Bioinformatics* 70: e102. <https://doi.org/10.1002/cpbi.102>.
- Richter, M., R. Rossello-Mora, F. Oliver Glockner, and J. Peplies. 2016. JSpeciesWS: A web server for prokaryotic species circumscription based on pairwise genome comparison. *Bioinformatics* 32: 929–931. <https://doi.org/10.1093/bioinformatics/btv681>.
- Roy, R., M. Tiwari, G. Donelli, and V. Tiwari. 2018. Strategies for combating bacterial biofilms: A focus on anti-biofilm agents and their mechanisms of action. *Virulence* 9: 522–554. <https://doi.org/10.1080/21505594.2017.1313372>.
- Sheehan, G., A. Margalit, D. Sheehan, and K. Kavanagh. 2021. Proteomic profiling of bacterial and fungal induced immune priming in *Galleria mellonella* larvae. *Journal of Insect Physiology* 131: 104213. <https://doi.org/10.1016/j.jinphys.2021.104213>.
- Shi, Y., Y. Peng, Y. Zhang, Y. Chen, C. Zhang, X. Luo, Y. Chen, Z. Yuan, J. Chen, and Y. Gong. 2021. Safety and efficacy of a Phage, kpsk3, in an in vivo model of carbapenem-resistant hypermucoviscous klebsiella pneumoniae bacteremia. *Frontiers in Microbiology* 12: 613356. <https://doi.org/10.3389/fmicb.2021.613356>.
- Simpson, D.J., Sacher, J.C., and Szymanski, C.M., 2016. Development of an assay for the identification of receptor binding proteins from bacteriophages. *Viruses* 8. <https://doi.org/10.3390/v8010017>.
- Soontarach, R., O.F. Nwabor, and S.P. Voravuthikunchai. 2022. Interaction of lytic phage T1245 with antibiotics for enhancement of antibacterial and anti-biofilm efficacy against multidrug-resistant *Acinetobacter baumannii*. *Biofouling* 38: 994–1005. <https://doi.org/10.1080/08927014.2022.2163479>.
- Sullivan, M.J., N.K. Petty, and S.A. Beatson. 2011. Easyfig: A genome comparison visualizer. *Bioinformatics* 27: 1009–1010. <https://doi.org/10.1093/bioinformatics/btr039>.
- Van Belleghem, J.D., Clement, F., Merabishvili, M., Lavigne, R., and M. Vanechoutte. 2017. Pro- and anti-inflammatory responses of peripheral blood mononuclear cells induced by *Staphylococcus aureus* and *Pseudomonas aeruginosa* phages. *Scientific Reports-Uk* 7. <https://doi.org/10.1038/s41598-017-08336-9>.
- Wang, L., T. Tkhilashvili, B. Bernal Andres, A. Trampuz, and M. Gonzalez Moreno. 2020. Bacteriophage-antibiotic combinations against ciprofloxacin/ceftriaxone-resistant *Escherichia coli* in vitro and in an experimental *Galleria mellonella* model. *International Journal of Antimicrobial Agents* 56: 106200. <https://doi.org/10.1016/j.ijantimicag.2020.106200>.
- Waters, E.M., D.R. Neill, B. Kaman, J.S. Sahota, M.R.J. Clokie, C. Winstanley, and A. Kadioglu. 2017. Phage therapy is highly effective against chronic lung infections with *Pseudomonas aeruginosa*. *Thorax* 72: 666–667. <https://doi.org/10.1136/thoraxjnl-2016-209265>.
- Wu, G., and Y. Yi. 2016. Haemocoel injection of PirA(1)B(1) to *Galleria mellonella* larvae leads to disruption of the haemocyte immune functions. *Science and Reports* 6: 34996. <https://doi.org/10.1038/srep34996>.
- Wu, G., Z. Zhao, C. Liu, and L. Qiu. 2014. Priming *Galleria mellonella* (Lepidoptera: Pyralidae) larvae with heat-killed bacterial cells induced an enhanced immune protection against *Photobacterium luminescens* TT01 and the role of innate immunity in the process. *Journal of Economic Entomology* 107: 559–569. <https://doi.org/10.1603/ec13455>.
- Wu, G., Y. Yi, Y. Lv, M. Li, J. Wang, and L. Qiu. 2015. The lipopolysaccharide (LPS) of *Photobacterium luminescens* TT01 can elicit dose- and time-dependent immune priming in *Galleria mellonella* larvae. *Journal of Invertebrate Pathology* 127: 63–72. <https://doi.org/10.1016/j.jip.2015.03.007>.
- Wu, G., Y. Yi, J. Sun, M. Li, and L. Qiu. 2015. No evidence for priming response in *Galleria mellonella* larvae exposed to toxin protein PirA2B2 from *Photobacterium luminescens* TT01: An association with the inhibition of the host cellular immunity. *Vaccine* 33: 6307–6313. <https://doi.org/10.1016/j.vaccine.2015.09.046>.
- Wu, G., L. Xu, and Y. Yi. 2016. *Galleria mellonella* larvae are capable of sensing the extent of priming agent and mounting proportional cellular and humoral immune responses. *Immunology Letters* 174: 45–52. <https://doi.org/10.1016/j.imlet.2016.04.013>.
- Xu, Y., X. Yu, Y. Gu, X. Huang, G. Liu, and X. Liu. 2018. Characterization and genomic study of phage vB_EcoS-B2 infecting multidrug-resistant *Escherichia coli*. *Frontiers in Microbiology* 9: 793. <https://doi.org/10.3389/fmicb.2018.00793>.
- Yin, S., G. Huang, Y. Zhang, B. Jiang, Z. Yang, Z. Dong, B. You, Z. Yuan, F. Hu, Y. Zhao, and Y. Peng. 2017. Phage Abp1 rescues human cells and mice from infection by pan-drug resistant *Acinetobacter baumannii*. *Cellular Physiology and Biochemistry* 44: 2337–2345. <https://doi.org/10.1159/000486117>.
- Zalis, E.A., Nuxoll, A.S., Manuse, S., Clair, G., Radlinski, L.C., Conlon, B.P., Adkins, J., and Lewis, K., 2019. Stochastic variation in expression of the tricarboxylic acid cycle produces persister cells. *mBio* 10. <https://doi.org/10.1128/mBio.01930-19>.